Proceedings RootS25
3rd International Workshop on Soil-Vegetation-Atmosphere Interaction
Boldrin D, Cecconi M, Cotecchia F, Leung A, Pedone G, Perrini P, Romero E, Tagarelli V, Zdravković L (eds)
ISSN: 3107-300X
© Authors: All rights reserved, 2025
doi: doi.org/10.53243/RootS2025-57

Capacity-limited infiltration in unsaturated slopes with root uptake: a semi-implicit 1D Richards model with Reduced-Order HM Storage

G. Cardile[1], N. Moraci[1]

[1]*Mediterranea University of Reggio Calabria, Department of Civil Engineering, Energy, Environment and Materials (DICEAM), Italy*

ABSTRACT: Rainfall infiltration alters matric suction and shear strength in partially saturated slopes, necessitating rapid and robust tools to simulate short-term transients during intense storms. This study proposes a 1D, slope-aligned model that solves a Gardner-type Richards equation with a depth-dependent root-uptake sink. A reduced-order, storage-only hydro-mechanical (HM) coupling is adopted: a lumped suction-based stiffness augments hydraulic storage and updates void ratio/porosity, thereby modulating hydraulic conductivity K_S and the Gardner capillary-scaling parameter α. This retains first-order skeleton compressibility at negligible cost, deliberately avoiding a fully coupled mechanical equilibrium, and is suited to early-warning systems and extensive parametric studies. Time integration employs a semi-implicit Crank-Nicolson (CN) scheme with an explicit half-step predictor, which controls local transients without requiring nonlinear iterations. In the simulated case, rainfall is applied in six-hour blocks; the testbed consists of a 2 m homogeneous colluvial layer over a far less permeable substratum. The parametric analysis targets silty-range K_S and rainfall intensity RI; within literature-based root-uptake ranges (T_R), vegetation effects are minor over 24–48 h. Across cases, K_S and RI govern wetting-front advance and the rate/timing of suction change. The framework delivers rapid forecasts of pressure head and infiltration depth, with diagnostics of boundary fluxes, storage, and HM contributions.

Keywords: Shallow landslides; Unsaturated flow; Richards equation; Infiltration; Lumped hydro-mechanical coupling

1 INTRODUCTION

Rainfall-induced transients reshape matric suction and effective stresses in unsaturated slopes and are central to shallow-failure inception (Cecconi et al., 2025; Pisano and Cardile, 2023). While multidimensional solvers are available, 1D slope-normal models remain valuable for fast forecasting (Conte and Troncone, 2012; Farthing and Ogden, 2017), parametric screening, and design comparison, provided that vegetation and suction–strength coupling are represented consistently and at a low computational cost.

The study casts the flow as a Gardner-type Richards equation with a depth-dependent root-uptake sink in slope-aligned coordinates. A reduced-order, storage-only hydro-mechanical (HM) coupling augments hydraulic storage with a lumped suction-based stiffness and updates void ratio/porosity, which in turn modulates K_s (Kozeny–Carman type scaling) and mildly adjusts α. This retains first-order skeleton compressibility without solving mechanical equilibrium, which suits early-warning systems (Mirus et al., 2025) and large-scale parametric studies. Time integration employs a semi-implicit Crank–Nicolson (CN) scheme (Crank and Nicolson, 1947) with an explicit half-step predictor and two lightweight safeguards (Δh-bounded rollback and a per-step mass-balance check) to control local transients without nonlinear iterations. Rainfall is applied in six-hour ON/OFF blocks with a capacity-limited surface boundary, based on the harmonic mean of the two nodal conductivities adjacent to the top face, and evaluated at the CN mid-step. This approach smooths transitions and avoids artificial flux spikes.

The testbed is a common shallow-landslide setting: a 2 m homogeneous colluvial layer (silty soils, clayey to sandy) over a far less permeable substratum, where infiltration accumulates at the base and saturation initiates at the bottom, migrating upward. The parametric analysis focuses on K_s (silty range), rainfall intensity RI and vegetation transpiration rates T_R.

2 PROBLEM SETTING AND ASSUMPTIONS

Let z^* be the slope-normal coordinate (positive downward) and β the slope angle. Under the infinite-slope idealisation, flow is one-dimensional along z^*; pore water is incompressible, the skeleton compressible.

In the Fredlund–Rahardjo (Fredlund and Rahardjo, 1993) framework, we distinguish two volume-change indices: the matric-suction index C_m and the net-stress index governing void-ratio updates (here represented by the saturated C_C.

The domain consists of a 2 m homogeneous layer over a low-permeability contact. The basal boundary is no-

flux, allowing rainfall to induce saturation within the upper layer. Unsaturated hydraulics follow Gardner's laws $k(h)=K_s e^{\alpha h}$ and $\theta(h)=\theta_r+(\theta_s+\theta_r)e^{\alpha h}$, where θ_r is the residual volumetric water content, $\theta_s=n=e/(1+e)$ is the saturated water content, K_S is the local saturated conductivity, and α is Gardner's soil-texture-dependent parameter (L^{-1}). Effective saturation is thus $S_e=e^{\alpha h}\in[0,1]$.

A macroscopic root-uptake sink represents vegetation (Bachofen et al., 2024) confined to $0\le z^*\le L_1$.

3 GOVERNING EQUATION AND BOUNDARY CONDITIONS

In slope-normal form, the governing equation for pressure head $h(z^*,t)$ is a variable-coefficient Richards equation in conservative form,

$$M(h,e)\frac{\partial h}{\partial t}=\frac{\partial h}{\partial z^*}\left[k(h,e)\left(\frac{\partial h}{\partial z^*}-\cos\beta\right)\right]-S(z^*,h) \qquad (1)$$

where the storage $M(h,e)$ is the sum of a hydraulic part and a lumped *HM* part: $M(h,e)=M_{hyd}(h,n)+M_{HM}(h,e)$.

The hydraulic contribution derives from $\partial\theta/\partial h$ and, neglecting $\partial n/\partial h$ within a time step as in the code, is well approximated by $M_{hyd}(h,n)\cong(n-\theta_r)\cdot\alpha(n)\cdot e^{\alpha(n)h}$. The reduced-order hydro-mechanical correction is introduced as $M_{HM}(h,e)=\gamma_w\alpha_C/H_{ms}(h,e)$, where H_{ms} is a suction-based stiffness and $\alpha_C\in[0,1]$ is a weighting factor (Fredlund and Rahardjo, 1993). The volume change index with respect to matric suction C_m supplies the suction-related storage in M_{HM}, whereas the C_C (volume change index for the virgin compression curve, used here as a proxy for the net-stress swelling index) parameterises e–log σ' update that feeds back to K_S and α. The Darcy flux in the rotated frame, projected along the slope-normal direction, is $q=k(h,e)\left[\partial h/\partial z^*-\cos\beta\right]$ (positive downward).

Vegetation is represented by a depth-dependent root-water-uptake sink term $S(z^*,h)=T_R W_r(z^*)f(h)$ acting within a rooted layer of thickness L_1. T_R is the transpiration demand; a triangular normalised vertical weighting $W_r(z^*)=2(L_1-z^*)/L_1^2$ for $0\le z^*\le L_1$ and zero below has been used, with a hydraulic activation $f(h)\in[0,1]$ that increases monotonically with $e^{\alpha h}$.

The partial differential equation was numerically solved using the finite difference Crank–Nicolson method (Crank and Nicolson, 1947), using a semi-implicit scheme with an explicit half-step predictor (Hundsdorfer and Verwer, 2003; Morton and Mayers, 2005).

At the surface, rainfall is set in six-hour ON/OFF blocks (for 48h) and the applied inflow is limited by the near-surface hydraulic capacity (Morbidelli et al., 2018) computed using the harmonic mean of the top-face conductivities (Berardi et al., 2018; Eymard et al., 2000) and evaluated at the Crank–Nicolson (CN) mid-step; no ponding is allowed ($h\le 0$). The base is no-flux ($\partial h/\partial z^*=\cos\beta$). Head and flux are continuous across the root-layer interface.

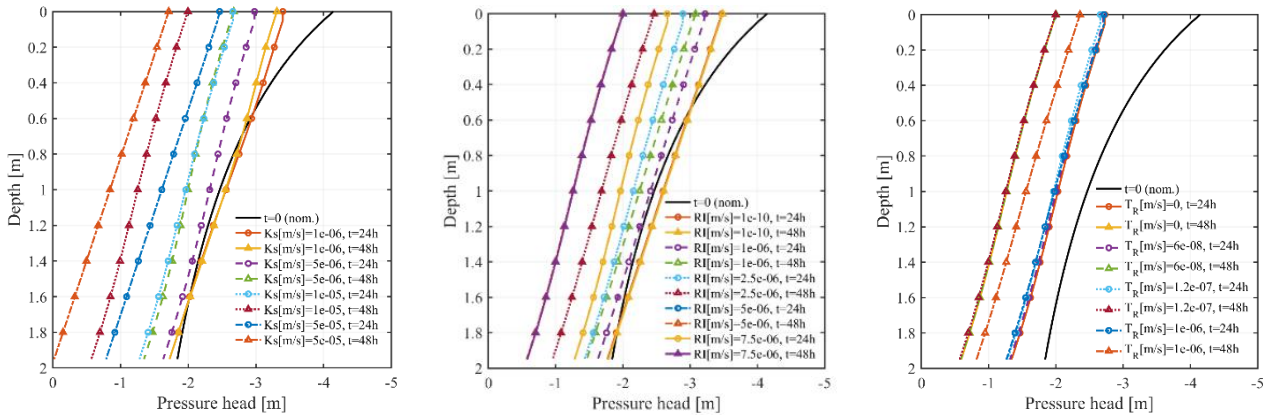
4 NUMERICAL METHOD (SEMI-IMPLICIT CRANK–NICOLSON)

Spatial operators are discretised on a uniform z^* grid with centred differences in conservative form; face conductivities use harmonic means for robustness. Time marching adopts Crank–Nicolson ($\vartheta=0.5$) realised through a predictor–corrector: an explicit half-step provides mid-step coefficients (unsaturated k, sink, and storage), followed by the CN update, thereby preserving second-order behaviour without Newton iterations. Two safeguards ensure robustness at negligible cost: (i) a Δh guard that triggers a single rollback to $\Delta t/2$ when $\max_i|h_i^{j+1}-h_i^j|$ exceeds a small threshold; (ii) a per-step mass-balance check (Celia et al., 1990) comparing storage change with net inflow minus uptake, likewise enabling one rollback if the relative error exceeds 0.5%. Only accepted steps refresh e, n, K_S, α, S_e. This design preserves second-order accuracy for smooth transients, stabilises ON/OFF transitions via the capacity-limited boundary, and remains computationally light for forecasting and parametric studies.

5 RESULTS OF THE PARAMETRIC ANALYSIS

The paper presents three one-factor-at-a-time parameter sweeps, varying saturated hydraulic conductivity K_S, rainfall intensity (RI), and transpiration demand T_R while holding all other inputs at their nominal values (2 m homogeneous layer over a low-permeability base; slope angle $\beta=30°$; Gardner parameter $\alpha=0.50$ m^{-1}; $T_R=1.2\times10^{-7}$ m s^{-1} with rooted layer $L_1=1$ m; $K_S=10^{-5}$ m s^{-1}, $RI=5\times10^{-6}$ m s^{-1} with capacity-limited surface boundary; Poisson's ratio $\mu=0.3$; mechanical compressibility index $C_m=0.05$; initial void ratio $e_0=0.8$; compression index $C_C=0.2$; initial degrees of saturation $S_r^{top}(t=0)=0.25$ and $S_r^{bottom}(t=0)=0.5$).

Figure 1 collects pressure-head profiles $h(z^*)$ at $t=24$ and $t=48$ h for each sweep: panel (a) varies $K_s\in[10^{-6}, 5\times10^{-6}, 10^{-5}, 5\times10^{-5}]$ m s^{-1}; panel (b) varies $RI\in[10^{-10}, 10^{-6}, 2.5\times10^{-6}, 5\times10^{-6}, 7.5\times10^{-6}]$ m s^{-1}; panel (c) varies $T_R\in[0.6\times10^{-8}, 1.2\times10^{-7}, 10^{-6}]$ m s^{-1}. The conductivity parametric analysis (Fig. 1a) shows the clearest control on infiltration depth. Increasing K_S shifts the profiles toward higher pressure heads (less negative h) throughout the column. It accelerates the downward progression of the wetting front over 24–48 h, with earlier development of a transient "perched" water table formed above the base. This behaviour is expected because larger K_S raises



(a) (b) (c)

Figure 1. Parametric analysis. Pressure-head profiles at selected times. (a) K_S (initial saturated conductivity at the top) variability; (b) rain intensity variability RI; (c) vegetation transpiration demand T_R variability (with L_l=1 m)

the near-surface capacity and reduces flow resistance along the column; once K_S is sufficiently large, the inflow becomes rainfall-limited rather than capacity-limited.

At $z*$=0.5 m, the reference suction heads are $\psi=-h$=3.02 m at 24 h and ψ=2.9 m at 48 h (s≈29.7 and 28.8 kPa). Increasing K_S from 10^{-6} to 5×10^{-6}, 10^{-5}, and 5×10^{-5} m s^{-1} produces a monotonic reduction of suction and a deeper, faster wetting response. At 24 h, the suction head at 0.5 m decreases by 13%, 24%, and 32%, corresponding to a suction variation of Δs=−3.8, −7.1, −9.6 kPa. By 48 h the reductions strengthen to 22%, 46%, and 56%, i.e. Δs=−6.3, −13.16, −16.26 kPa.

At the base z^*=2 m, which is critical for the potential formation of a transient perched water table and potential landslide failure onset, the trend is stark. Relative to the reference (ψ≈1.73 m at 24–48 h; s≈16.9 kPa), at 24 h the suction head decreases by −5%, −26%, and −54% (Δs= −0.92, −4.36, −9.20 kPa). At 48 h, the changes reach −22%, −67%, and −99%, i.e. Δs=−3.70, −11.32, −16.70 kPa. In absolute terms, for K_S =5×10−5 m s^{-1} the base evolves from h=−1.73 m (reference) to h= −0.02 m by 48 h (s≈0.23 kPa), indicating near-saturated conditions at the contact with the low-permeability substratum.

The rainfall-intensity sweep (Fig. 1b) shows a monotonic response up to the capacity limit: increasing *RI* strengthens suction reductions and deepens penetration until the near-surface capacity is reached; beyond that threshold, larger *RI* no longer increases infiltration proportionally, so the RI = 5×10^{-6} and 7.5×10^{-6} m s^{-1} curves are coincident. At z*=1 m, relative to the very-low input (RI =10^{-10} m s^{-1}), suction reductions are 7%, 17%, and 24% at 24 h (Δs=−1.84,−4.34,−6.23 kPa) and 14%, 35%, and 52% at 48 h (Δs=−3.55,−9.09,−13.29 kPa) for RI =10^{-6}, 2.5×10^{-6}, 5×10^{-6} m s^{-1}, with no further change at 7.5×10^{-6} m s^{-1}. At the bottom (z^*=2 m), reductions are 8%, 19%, and 28% at 24 h (Δs=−1.40, −3.33, −4.80 kPa) and 18%, 47%, and 68% at 48 h (Δs=−3.13, −8.14, −11.90 kPa), again saturating between 5 and 7.5×10^{-6} m s^{-1}.

The transpiration sweep (Fig. 1c) indicates that vegetation has a minor hydraulic effect over 24–48 h for literature-range values $T_R \le 1.2\times10^{-7}$ m s^{-1} (Allen et al., 1998; Gao et al., 2022; Raz-Yaseef et al., 2012; Zhu and Zhang, 2015), encompassing typical growing-season rates ~1–5 mm day^{-1} and occasional high-demand episodes ~6–10 mm day^{-1}. The pressure-head profiles for T_R=0 and for the parametric values are indistinguishable at the plotting scale. Only the stress-test T_R=10^{-6} m s^{-1} produces a visible near-surface attenuation of suction losses, confined to the rooted layer and with negligible impact at depth.

At z^*=0.5 m, in the reference case (T_R=0), the suction heads are ψ=2.37 m at 24 h and ψ=1.60 m at 48 h, i.e. s=23.3 and 15.7 kPa. For literature-range values of T_R, the impact over 24–48 h is small. With T_R=6×10^{-8} m s^{-1}, the change at 24 h is −1%, corresponding to Δs=−0.26 kPa, and it is essentially null at 48 h. With T_R=1.2×10^{-7} m s^{-1}, the changes are −3% at 4 h (Δs=−0.69 kPa) and −1% at 48 h (Δs=−0.08 kPa). Only the numerical stress test T_R=10^{-6} m s^{-1} yields a marked response: at 48 h the suction head increases by ~21%, with Δs=+3.31 kPa at 0.5 m. Within the realistic range of T_R, however, differences remain within a few per cent (and within ≲0.7 kPa at 0.5 m), confirming a minor hydraulic role over 24–48 h compared with K_S and rainfall intensity.

To complement the space–time and pointwise diagnostics, a comparable metric is introduced across all scenarios: the depth-averaged suction head, $\bar{\psi} = L^{-1}\int_0^L \left[-h\left(z^*,t\right)\right]\cdot dz$ [m], which is proportional to the column-averaged matric suction [kPa]. A decrease in $\bar{\psi}$ denotes loss of suction and a wetter column. For each parametric analysis, the authors report changes relative to a parametric-specific reference case.

For the saturated hydraulic conductivity sweep (reference K_S =10^{-6} m s^{-1}), increasing K_S produces a clear, monotonic reduction in $\bar{\psi}$. At 24 h, the depth-averaged suction head decreases by approximately 10%, 23%,

and 37% for K_S =5×10^{-6}, 10^{-5}, 5×10^{-5} m s^{-1}, respectively, corresponding to column-mean suction changes Δs_{mean}≈−2.50, −5.87, and −9.34 kPa. By 48 h the reductions intensify to about 21%, 50%, and 66% (Δs_{mean}≈−5.24, −12.44, −16.46 kPa). These data confirm that permeability controls both the magnitude and pace of wetting in this configuration.

For the rainfall-intensity sweep (referenced to RI=10^{-10} ≅ 0 m s^{-1}), $\bar{\psi}$ again declines markedly as RI increases, but the response saturates once the capacity-limited surface boundary becomes active. At 24 h, increasing RI to 10^{-6}, 2.5×10^{-6}, 5×10^{-6} m s^{-1} reduces $\bar{\psi}$ by about 7%, 17%, and 24% (Δs_{mean}≈−1.85, −4.35, −6.24 kPa). In contrast, a further increase to 7.5×10^{-6} m s^{-1} yields no additional reduction, indicating that the near-surface hydraulic capacity is already limiting infiltration. By 48 h, the reductions reach roughly 14%, 35%, and 52% for 10^{-6}, 2.5×10^{-6}, 5×10^{-6} m s^{-1} (Δs_{mean}≈−3.55, −9.09, −13.29 kPa), with 7.5×10^{-6} m s^{-1} remaining indistinguishable from 5×10^{-6} m s^{-1}.

For the transpiration-demand sweep (reference T_R =0), vegetation effects on $\bar{\psi}$ are minor within literature-based ranges over 24–48 h. Using T_R =6×10^{-8} and 1.2×10^{-7} m s^{-1}, the depth-averaged suction head differs from the reference by only about 1% and 3% at 24 h and by 0% and 1% at 48 h. A noticeable signal appears only under the numerical stress test T_R =10^{-6} m s^{-1}: the 48 h $\bar{\psi}$ increases by about 23% (Δs_{mean}≈+2.86 kPa), indicating a substantially drier column driven by unrealistically high extraction.

6 CONCLUSIONS

The study provides a basis for comparing scenarios and for prioritising parameters in screening and early-warning applications. Operationally, the model can map forecasted rainfall blocks into timelines of suction loss and wetting-front depth; it can be initialised using in-situ measurements of shallow pressure head and volumetric water content to reduce uncertainty, and its outputs can be translated into simplified stability indicators to support threshold-based alerts.

Overall, across the explored space, K_S and rainfall intensity govern the advance of the wetting front, as well as the timing and magnitude of suction change. In contrast, realistic T_R values play a secondary role over the short horizons considered. Although the vegetation signal is modest in the present runs, this conclusion is specific to short (24–48 h) storm transients and to a hydraulic representation in which vegetation acts only through root uptake (transpiration). Over longer horizons (multi-day to seasonal), cumulative evapotranspiration can substantially dry the near-surface layer, lower antecedent water contents, and thereby delay subsequent wetting fronts and suction losses, effects that lie beyond the scope of the present analysis.

7 REFERENCES

Allen, R., Pereira, L., Smith, M. 1998. Crop Evapotranspiration, *Guidelines for Computing Crop Water Requirements*.

Bachofen, C., Tumber-Dávila, S.J., Mackay, D.S., McDowell, N.G., Carminati, A., Klein, T., Stocker, B.D., Mencucci-ni, M., Grossiord, C. 2024. Tree water uptake patterns across the globe, *New Phytologist* **242**, 1891-1910.

Berardi, M., Difonzo, F., Vurro, M., Lopez, L. 2018. The 1D Richards' equation in two layered soils: a Filippov approach to treat discontinuities, *Advances in Water Resources* **115**, 264-272.

Celia, M.A., Bouloutas, E.T., Zarba, R.L. 1990. A general mass-conservative numerical solution for the unsaturated flow equation, *Water Resources Research* **26**, 1483-1496.

Cecconi, M., Tagarelli, V., Cotecchia, F., et al. 2025. Soil-vegetation-atmosphere interaction for engineering applications: Recent multi-scale and multi-disciplinary insights, *Geomechanics for Energy and the Environment* **43**, 100723.

Conte, E., Troncone, A. 2012. A method for the analysis of soil slips triggered by rainfall, *Géotechnique* **62**, 187-192.

Crank, J., Nicolson, P. 1947. A practical method for numerical evaluation of solutions of partial differential equations of the heat-conduction type, *Mathematical Proceedings of the Cambridge Philosophical Society* **43**, 50-67.

Eymard, R., Thierry, G., Herbin, R. 2000. Finite Volume Methods, *Handbook of Numerical Analysis* **7**.

Farthing, M.W., Ogden, F.L. 2017. Numerical Solution of Richards' Equation: A Review of Advances and Challenges, *Soil Science Society of America Journal* **81**, 1257-1269.

Fredlund, D.G., Rahardjo, H. 1993. *Soil Mechanics for Unsaturated Soils*. John Wiley & Sons, Inc.

Gao, G., Wang, D., Zha, T., Wang, L., Fu, B. 2022. A global synthesis of transpiration rate and evapotranspiration partitioning in the shrub ecosystems, *Journal of Hydrology* **606**, 127417.

Hundsdorfer, W., Verwer, J. 2003. *Numerical Solution of Time-Dependent Advection-Diffusion-Reaction Equations*.

Mirus, B.B., Bogaard, T., Greco, R., Stähli, M. 2025. Invited perspectives: Integrating hydrologic information into the next generation of landslide early warning systems, *Nat. Hazards Earth Syst. Sci.* **25**, 169-182.

Morbidelli, R., Corradini, C., Saltalippi, C., Flammini, A., Dari, J., Govindaraju, R.S. 2018. Rainfall Infiltration Modeling: A Review, *Water* **10**, 1873.

Morton, K.W., Mayers, D.F. 2005. *Numerical Solution of Partial Differential Equations: An Introduction*, 2 ed. Cambridge University Press, Cambridge.

Pisano, M., Cardile, G. 2023. Probabilistic Analyses of Root-Reinforced Slopes Using Monte Carlo Simulation, *Geosciences* **13**, 75.

Raz-Yaseef, N., Yakir, D., Schiller, G., Cohen, S. 2012. Dynamics of evapotranspiration partitioning in a semi-arid forest as affected by temporal rainfall patterns, *Agricultural and Forest Meteorology* **157**, 77-85.

Zhu, H., Zhang, L.M. 2015. Evaluating suction profile in a vegetated slope considering uncertainty in transpiration, *Computers and Geotechnics* **63**, 112-120.